Cite as: N. Maksimovic *et al.*, *Science* 10.1126/science.aaz4566 (2021).

Evidence for a delocalization quantum phase transition without symmetry breaking in $CeCoIn_5$

Nikola Maksimovic[1,2]*, Daniel H. Eilbott[1,2], Tessa Cookmeyer[1,2], Fanghui Wan[1,2], Jan Rusz[5], Vikram Nagarajan[1,2], Shannon C. Haley[1,2], Eran Maniv[1,2], Amanda Gong[1,2], Stefano Faubel[1,2], Ian M. Hayes[1,2], Ali Bangura[4], John Singleton[3], Johanna C. Palmstrom[3], Laurel Winter[3], Ross McDonald[3], Sooyoung Jang[1,2], Ping Ai[2], Yi Lin[2], Samuel Ciocys[1,2], Jacob Gobbo[1,2], Yochai Werman[1,2], Peter M. Oppeneer[5], Ehud Altman[1,2], Alessandra Lanzara[1,2], James G. Analytis[1,2]*

[1]Department of Physics, University of California, Berkeley, Berkeley, CA 94720, USA. [2]Materials Sciences Division, Lawrence Berkeley National Laboratory, Berkeley, CA 94720, USA. [3]National High Magnetic Field Laboratory, Los Alamos, NM 97545, USA. [4]National High Magnetic Field Laboratory, Tallahassee, FL 32310, USA. [5]Department of Physics and Astronomy, Uppsala University, Box 516, S-75120 Uppsala, Sweden.

*Corresponding author. Email: nikola_maksimovic@berkeley.edu (N.M.); analytis@berkeley.edu (J.G.A.)

The study of quantum phase transitions that are not clearly associated with a broken symmetry is a major effort in condensed matter physics, particularly in the problem of high-temperature superconductivity where such transitions are thought to underlie the mechanism of superconductivity itself. In this study, we argue that the putative quantum critical point in the prototypical unconventional superconductor $CeCoIn_5$ is characterized by the delocalization of electrons in a transition that connect two Fermi surfaces of different volumes, with no apparent broken symmetry. Drawing on established theory of *f*-electron metals, we discuss an interpretation for such a transition that involves the fractionalization of spin and charge, a model which well-describes the anomalous transport behavior we measure in the Hall effect.

$CeCoIn_5$ is an *f*-electron metal with notable similarities to high-temperature superconducting copper-oxides, for example in crystal structure, transport properties, and unconventional superconductivity (*1*–*10*). Both sets of materials also exhibit signatures of a quantum phase transition (QPT), a phase transition induced by a non-thermal parameter, underlying the superconducting state. However, in many unconventional superconductors, it is unclear whether the underlying QPT can be understood in the conventional sense as separating phases with different symmetries. An exploration of unconventional types of QPTs, non-symmetry breaking (*11*) or weakly symmetry breaking (*12*, *13*), has therefore become a subject of intense study. In this work, we bring evidence that $CeCoIn_5$ is proximate to a quantum phase transition where the density of itinerant electrons changes apparently without breaking of symmetry. Established theory of *f*-electron metals provides a route to interpret such a transition.

At the microscopic level, *f*-electron metals such as $CeCoIn_5$ are described by a Kondo lattice model. Each cerium atom hosts a single *f* level valence electron which contributes a localized spin-1/2 moment. These local moments coexist with a sea of itinerant conduction electrons. In the conventional metallic ground state of the Kondo lattice, the *f*-electrons appear to become an integral part of the itinerant metal. In particular, they join the conduction electrons, contributing their full share to the total Fermi volume as prescribed by Luttinger's theorem (*14*). This phenomenon occurs through the formation of Kondo singlet correlations between the local *f* moments and the conduction electrons, which effectively hybridize the *f* level with the conduction bands.

A long-standing challenge has been to characterize a QPT in which the *f*-electrons recover their localized character and withdraw from the itinerant Fermi volume. Superficially, the remaining Fermi volume without *f*-electrons is in apparent violation of Luttinger's theorem. The loss of Fermi volume when *f*-electrons localize is therefore conventionally accompanied by a transition to a (antiferromagnetic) spin-density wave state, whereby Luttinger's theorem is recovered in the appropriately folded Brillouin zone associated with translational symmetry breaking (*15*–*19*). In this paper, we present Hall effect, quantum oscillation, and angle-resolved photoemission spectroscopy (ARPES) measurements of $CeCoIn_5$ with small levels of chemical substitution, and compare the experimental data to ab initio calculations. We find evidence for an *f*-electron delocalization QPT without symmetry breaking.

Figure 1A presents low-temperature measurements of the Hall resistivity, ρ_{xy}, versus magnetic field, H, for $CeCoIn_5$ samples with varying levels of cadmium (hole-doping) or tin (electron-doping), both of which substitute indium. The Hall coefficient, $R_H = \rho_{xy} / \mu_0 H$ can be used to estimate the net carrier density enclosed by the Fermi surface according to the formula (*20*)

$$n_{net} = \frac{1}{eR_H\left(H \to \infty\right)} \quad (1)$$

where n_{net} is the net carrier density—electrons minus holes. In multiple band metals such as $CeCoIn_5$, Eq. 1 only applies in the limit where high fields eliminate the effects of carrier mobility misbalances and R_H becomes field-independent (see (*21*) Section 3 for more details on the high-field limit). For each sample, we measure the high-field value of R_H at 0.5 K in order to approximate the net carrier density. Many of the traces shown in Fig. 1A appear to saturate at high fields, and fig. S4 (*21*) shows that evaluation of the high-field slope of ρ_{xy} is in good agreement with the high-field value of $\rho_{xy} / \mu_0 H$, suggesting that at these temperatures and fields the Hall coefficient is close to field-independent. In addition, select samples were measured in pulsed magnetic fields up to 75 T, as shown in Fig. 1B, where the Hall coefficient is field-independent over an extended field range; the extracted Hall coefficients from pulsed and continuous fields are in good agreement for these samples (Fig. 1C). Finally, our Hall coefficient measurements on pure $CeCoIn_5$ agree well with measurements at 20 mK where the Hall resistivity is completely linear in field (*22*). These facts together give confidence that our extracted Hall coefficient values can be interpreted as an approximate measurement of the net carrier density as described by Eq. 1.

Figure 1C shows the value of $1/eR_H$, approximating the net carrier density, extracted for samples with different levels of chemical substitution in continuous and pulsed magnetic fields. The carrier density of this material excluding the *f*-electron can be established using Hall resistivity measurements of $LaCoIn_5$ shown in Fig. 1B (its Hall coefficient is field-independent above 5 T at 1.8 K. See also fig. S3 (*21*)); $LaCoIn_5$ can be thought of as $CeCoIn_5$ without the *f*-electron. We find that the Hall coefficient of $CeCoIn_5$, evaluated either up to 60 Tesla or up to 14 Tesla at 0.5 K, is close to that of $LaCoIn_5$ (Fig. 1C). This suggests that the two materials have similar net carrier densities, implying that the *f*-electrons are close to localized in $CeCoIn_5$. With cadmium-substitution $1/eR_H$ remains close to that of $LaCoIn_5$, but with tin substitution increases to a value consistent with the addition of one itinerant electron per unit cell. Identifying the additional electron as the single cerium *f*-electron suggests that Sn-substitution induces a delocalization transition of the *f*-electrons. None of these samples show a finite-temperature phase transition other than superconductivity. Only in Cd substitution levels higher than 0.6% is an antiferromagnetic phase observed (fig. S1 (*21*)) (*23*). In addition, the specific heat capacity at moderate temperature remains constant across this substitution series (Fig. 1C); we will comment more on this later.

When the *f*-electrons delocalize, the Fermi surfaces are expected to reconstruct and increase in volume. The results of our density functional theory (DFT) calculations of the three Fermi surfaces comparing the (de)localized *f*-electron models are visualized in Fig. 2A (DFT calculation details are provided in (*21*) Section 1). In summary, according to the calculation *f*-electron delocalization causes the extended γ surface to disconnect into small ellipsoidal pockets at the Brillouin zone center and edge, and the γ pocket at the zone top (γ_Z) to disappear. Also, large extended surfaces α_Z and β_Z appear at the zone top, and the α and β cylinders expand slightly. In pure $CeCoIn_5$, previous angle-resolved photoemission (ARPES) data at 10-20 K are in better qualitative agreement with the localized *f*-electron model as α_Z and β_Z are absent, and γ_Z is present (*24*, *25*). However, the volumes of the α and β cylinders are slightly larger than those of the localized model (*24*–*26*), and the smaller γ Fermi surface seems to exhibit features of both the delocalized and localized models, being potentially disconnected (suggesting delocalized) but retaining γ_Z (suggesting localized) (*24*, *25*, *27*, *28*). These characteristics may point to a partially delocalized *f*-electron character in pure $CeCoIn_5$. This interpretation is also promoted by previous magnetic resonance (*29*) and photoemission studies (*24*, *30*, *31*). Note that our Hall effect measurements suggest that the *f*-electrons only weakly contribute to the Fermi volume of $CeCoIn_5$ even at 0.5 K, consistent with partially localized *f*-electrons in the low-temperature limit.

De Haas-van Alphen (dHvA) oscillations measure extremal areas of the Fermi surface perpendicular to the field direction, giving a probe of the Fermi surface structure at extremely low temperature. Here we compare our dHvA measurements of Sn-doped $CeCoIn_5$ and published data on pure $CeCoIn_5$ (*5*). As seen in Table 1 and Fig. 1C, the sizes of the α and β cylinder orbits in pure $CeCoIn_5$ are more consistent with the delocalized model, implying that *f*-electrons incorporate into these Fermi surface sheets. However, there do not appear to be additional frequencies associated with the α_Z and β_Z sheets of the delocalized model, and orbit β_2 increases as a function of tilt angle away from [001] (Fig. 2C), further suggesting that the β cylinder is fully connected in better qualitative agreement with the localized model. In the Sn-substituted sample, the sizes of the α and β cylinders change slightly compared to pure $CeCoIn_5$ (Table 1). In addition, an oscillation of about 16 kT appears for two field angles near [001]. This oscillation does not appear to be harmonically related to the α_{1-3} branches, and its frequency and angle-dependence agree well with a predicted orbit on α_Z of our delocalized model calculations. Furthermore, 1.2 kT and 2 kT frequencies for field angles near [001] are indicative of holes in the β cylinder (Fig. 2A), and, a branch of the β_2 cylinder orbit appears to decrease as a function of tilt angle from [001] in better agreement with the delocalized model (Fig. 1C), further suggesting that holes develop in the β cylinder. Finally, possible low frequency oscillations <800 T at several angles, which seem to be present in pure $CeCoIn_5$ over certain angular ranges as well, are most naturally assigned to small

γ-ellipsoids (Fig. 2C), but could also originate from the γ_Z sheet. Table 1 summarizes the frequency assignments based on comparison to DFT calculations, which suggests that the α_Z and β_Z sheets are present in the Fermi surface of the Sn-substituted sample. From dHvA, it is not possible to conclusively say whether these sheets are absent in pure $CeCoIn_5$ at low temperature because the orbit frequencies on α_Z and β_Z are sensitive to the precise structure of these Fermi surfaces. Nevertheless, the comparison shown in Table 1 is indicative of a Fermi surface reconstruction induced by Sn-substitution.

Our ARPES measurements corroborate the dHvA evidence for a Fermi surface reconstruction. Figure 3 compares Fermi surface maps at the Brillouin zone top in pure $CeCoIn_5$ and 3% Sn-substituted $CeCoIn_5$ at 10 K (additional data are provided in (*21*) Section 9). Our data on pure $CeCoIn_5$ agrees well with previous reports. The cylindrical Fermi surfaces centered at the zone corners are visible. Bright spots near the Z point are probably signatures of the γ_Z Fermi surface, as discussed in Refs. (*27*, *31*). In the 3% Sn-substituted sample, we observe enhanced intensity at the R point of the Brillouin zone relative to the pure material, as well as a qualitative change in structure near Z. Overall it appears that the electronic structure changes with Sn-substitution, with a sharp cross-shaped structure emerging in the RZA plane which resembles α_Z or β_Z of our delocalized model calculations (α and β bands nearly overlap along this cut, and as such they may be difficult to distinguish from one another in ARPES). Weak features appear at the R point in pure $CeCoIn_5$ as well, potentially indicating that incoherent states exist at the R point—these states may exist because of the partially delocalized *f*-electron character in the pure material. In Fig. 3C, we explore the temperature-dependence of these Fermi surface sheets via the ARPES intensity at the R point. The relative intensity at R increases in the Sn-substituted sample upon decreasing temperature below about 90 K with the onset of *f*/conduction hybridization (see also fig. S16 (*21*)). In the pure material, the R point spectral weight is relatively constant down to 10 K. This comparison suggests that the Fermi surface sheet in 3% Sn-doped $CeCoIn_5$ emerges, or is made relatively more coherent, because of enhanced *f*/conduction electron hybridization induced by Sn-substitution.

One way to view *f*-electron delocalization is as a result of Kondo hybridization between the *f* level and conduction electrons. Although there are reports of hybridization developing below about 45 Kelvin in pure $CeCoIn_5$ (*27*) and Cd-doped $CeCoIn_5$ (*32*) resulting in a detectable *f*-electron contribution to the Fermi surface, we find that the low-temperature carrier density of these materials is consistent with predominantly localized *f*-electrons (Fig. 1). In contrast to the pure material, the net carrier density of Sn-substituted samples appears to include the *f*-electrons (Fig. 1C). This change coincides with signatures of new Fermi surface sheets (Fig. 3 and Table 1), which seem to agree well with predicted Fermi surfaces unique to the delocalized *f*-electron DFT model (Fig. 2A). Taken together, these data suggest that Sn-substitution of $CeCoIn_5$ induces a Fermi volume changing transition between a phase with predominantly localized *f*-electrons to one with a delocalized character. This transition could be attributed to an enhancement of the Kondo coupling induced by electron doping (*25*, *33*, *34*). High magnetic fields may compete with the Kondo coupling by polarizing the *f*-electrons, but notably the Hall resistivity remains linear up to 73 T (Fig. 1B), so it seems likely that higher fields are required to induce a complete breakdown of Kondo hybridization.

A delocalization transition is a reasonable scenario from the perspective of doping-tuned Kondo coupling. Because of the constraints imposed by Luttinger's theorem, the reduction in Fermi volume in the more localized *f*-electron regime is expected to coincide with antiferromagnetic order where the Brillouin zone is reduced (*15*). It is however hard to reconcile this scenario with the data because the transition to antiferromagnetism is seen only around Cd doping of 0.6% (*23*), considerably removed from the suggested delocalization transition induced by Sn-substitution (Fig. 1C). Furthermore, magnetic order has never been observed in native $CeCoIn_5$ or Sn-substituted $CeCoIn_5$ (*6*, *25*, *33*, *34*), and the ARPES and dHvA data suggest that the Brillouin zone is essentially unchanged by Sn-substitution. An alternative possibility is the formation of a fractionalized phase in the more localized *f*-electron regime (*11*). In this theoretically predicted phase, the *f*-electron charge localizes to the cerium site, reducing the Fermi volume, while the spin excitations of the *f* moments remain itinerant and form a charge neutral Fermi surface (*11*). We can speculate that the specific heat remains constant across the substitution series (Fig. 1C) owing to the presence of such a neutral Fermi surface, which conserves the fermionic degrees of freedom of the system even when the density of itinerant electrons appears to increase. One may also expect quantum fluctuations associated with a delocalization transition to enhance the specific heat coefficient. Such an enhancement has been observed as a function of decreasing temperature below 2 K in pure $CeCoIn_5$ (*2*). The confinement of these effects to <2 K temperatures could explain why we do not detect singular behavior in C/T at 4 K across the substitution series.

Our calculations of the Hall conductivity of such a fractionalized phase capture several distinctive aspects of the low-field Hall coefficient in this material. In the simplest description of the fractionalized Fermi liquid, the *f*-electron separates into a fermionic spinon carrying its spin, and a gapped bosonic mode, in this case a valence fluctuation, carrying its charge. *f*-electron delocalization can be identified with the closing of the boson gap. Near this transition, the electrical conductivity has contributions from the fermionic spinons,

the charged bosons and the conduction electrons. The spinon and the bosons should be added in series (*35*). The boson's resistivity will then dominate owing to their much smaller number, and we therefore neglect the spinon contribution. Adding to this the resistivity of the conduction band in parallel gives:

$$R_H = R_H^c \frac{\sigma_c^2}{(\sigma_{\rm tot})^2} + \frac{1}{\mu_0 H} \frac{\sigma_{xy}^b}{(\sigma_{\rm tot})^2} \quad (2)$$

where σ_c and R_H^c are the longitudinal conductivity and Hall coefficient of the conduction electrons, respectively, and σ_{xy}^b is the Hall conductivity of the bosonic valence fluctuations. The total conductivity is $\sigma_{\rm tot}$. In our calculation, we consider two processes that contribute to the scattering rate of the valence fluctuations. One process is provided by the internal gauge field (*11*). The other mechanism is scattering on the doped ions, which grows linearly with the doping level (see fig. S5 (*21*)). One may expect an enhancement of the low-field Hall coefficient stemming from the second term in Eq. 2 caused by the singular behavior of the valence fluctuations when the boson gap closes. This expectation is corroborated by a semi-classical Boltzmann analysis, the details of which are given in (*21*) Section 7. As shown in Fig. 4, the results of the calculation of the conductivity in this model give good agreement with the measured Hall coefficient as a function of temperature, doping level, and magnetic field with the assumption that pure $CeCoIn_5$ is the sample closest to the delocalization transition. The results shown in Fig. 4B are obtained from a calculation of σ_{xy}^b, and converted to a Hall coefficient using the physical resistivity of the system $1/\sigma_{\rm tot} = \rho_{xx} \sim T$ as observed in the experiment over the relevant temperature range. A more complete description of the longitudinal resistivity in this model will be the subject of future work.

We emphasize that the experimental observations seen in Fig. 4 are difficult to reconcile with more conventional transport models. From the point of view of band theory, the low-field R_H is proportional to the carrier density of the most mobile carriers (*20*), so it is surprising that R_H has such a strong temperature-dependence with a peak at finite temperature, and retains the same sign and uniformly decreases with either hole or electron doping. In addition, the observed symmetric-in-doping Hall coefficient cannot be readily attributed to disorder scattering induced by substitution, as we find that disordering the material by other means, substituting lanthanum for cerium, has a relatively small effect on the low-field R_H (see fig. S6 (*21*)). These key features of the experimental transport data are captured by the valence fluctuation model described above.

The present study provides evidence that $CeCoIn_5$ exists near a quantum phase transition associated with the delocalization of *f*-electron charge. The absence of evidence for symmetry breaking around this transition opens the possibility for the fractionalization of *f*-electrons into separate spin and charge degrees of freedom. Although our conductivity calculations support this theoretical picture, direct evidence for such fractionalized electrons is desirable, and may be possible with inelastic neutron measurements (*36*) or Josephson tunneling experiments (*37*). On a final note, recent experiments on cuprate high-temperature superconductors find evidence for a Fermi surface reconstruction where the localized charge of the Mott insulator gradually delocalizes over a certain oxygen doping range near the endpoint of the pseudogap phase (sometimes referred to as a p to $1+p$ transition (*38*)). We have presented evidence for an analogous transition in an *f*-electron metal. It is possible that such a quantum phase transition underlies some of the similarities between $CeCoIn_5$ and cuprate superconductors (*1–9*), and perhaps our work may help guide interpretation of these recent results on cuprates.

REFERENCES AND NOTES

1. C. Petrovic, P. G. Pagliuso, M. F. Hundley, R. Movshovich, J. L. Sarrao, J. D. Thompson, Z. Fisk, P. Monthoux, Heavy-fermion superconductivity in $CeCoIn_5$ at 2.3 K. *J. Phys. Condens. Matter* **13**, L337 (2001). doi:10.1088/0953-8984/13/17/103
2. A. Bianchi, R. Movshovich, I. Vekhter, P. G. Pagliuso, J. L. Sarrao, Avoided antiferromagnetic order and quantum critical point in $CeCoIn_5$. *Phys. Rev. Lett.* **91**, 257001 (2003). doi:10.1103/PhysRevLett.91.257001 Medline
3. J. Paglione, M. A. Tanatar, D. G. Hawthorn, E. Boaknin, R. W. Hill, F. Ronning, M. Sutherland, L. Taillefer, C. Petrovic, P. C. Canfield, Field-induced quantum critical point in $CeCoIn_5$. *Phys. Rev. Lett.* **91**, 246405 (2003). doi:10.1103/PhysRevLett.91.246405 Medline
4. Y. Nakajima, H. Shishido, K. Izawa, Y. Matsuda, H. Kontani, K. Behnia, H. Hedo, Y. Uwatoko, T. Matsumoto, R. Settai, Y. Onuki, Unusual Hall effect in quasi two-dimensional strongly correlated metal $CeCoIn_5$. *Phys. C* **460-462**, 680–681 (2007). doi:10.1016/j.physc.2007.03.082
5. R. Settai, H. Shishido, S. Ikeda, Y. Murakawa, M. Nakashima, D. Aoki, Y. Haga, H. Harima, Y. Onuki, Quasi-two-dimensional Fermi surfaces and the de Haas-van Alphen oscillation in both the normal and superconducting mixed states of $CeCoIn_5$. *J. Phys. Condens. Matter* **13**, L627 (2001). doi:10.1088/0953-8984/13/27/103
6. Y. Kohori, Y. Yamato, Y. Iwamoto, T. Kohara, E. D. Bauer, M. B. Maple, J. L. Sarrao, NMR and NQR studies of the heavy fermion superconductors $CeTIn_5$ (T = Co and Ir). *Phys. Rev. B* **64**, 134526 (2001). doi:10.1103/PhysRevB.64.134526
7. V. A. Sidorov, M. Nicklas, P. G. Pagliuso, J. L. Sarrao, Y. Bang, A. V. Balatsky, J. D. Thompson, Superconductivity and quantum criticality in $CeCoIn_5$. *Phys. Rev. Lett.* **89**, 157004 (2002). doi:10.1103/PhysRevLett.89.157004 Medline
8. B. B. Zhou, S. Misra, E. H. da Silva Neto, P. Aynajian, R. E. Baumbach, J. D. Thompson, E. D. Bauer, A. Yazdani, Visualizing nodal heavy fermion superconductivity in $CeCoIn_5$. *Nat. Phys.* **9**, 474–479 (2013). doi:10.1038/nphys2672
9. C. Stock, C. Broholm, J. Hudis, H. J. Kang, C. Petrovic, Spin resonance in the d-wave superconductor $CeCoIn_5$. *Phys. Rev. Lett.* **100**, 087001 (2008). doi:10.1103/PhysRevLett.100.087001 Medline
10. Y. Tokiwa, E. D. Bauer, P. Gegenwart, Zero-field quantum critical point in $CeCoIn_5$. *Phys. Rev. Lett.* **111**, 107003 (2013). doi:10.1103/PhysRevLett.111.107003 Medline
11. T. Senthil, M. Vojta, S. Sachdev, Weak magnetism and non-Fermi liquids near heavy-fermion critical points. *Phys. Rev. B* **69**, 035111 (2004). doi:10.1103/PhysRevB.69.035111
12. C. M. Varma, Theory of the pseudogap state of the cuprates. *Phys. Rev. B* **73**, 155113 (2006). doi:10.1103/PhysRevB.73.155113

13. S. Lederer, Y. Schattner, E. Berg, S. A. Kivelson, Superconductivity and non-Fermi liquid behavior near a nematic quantum critical point. *Proc. Natl. Acad. Sci. U.S.A.* **114**, 4905–4910 (2017). doi:10.1073/pnas.1620651114 Medline
14. M. Oshikawa, Topological approach to Luttinger's theorem and the fermi surface of a kondo lattice. *Phys. Rev. Lett.* **84**, 3370–3373 (2000). doi:10.1103/PhysRevLett.84.3370 Medline
15. Q. Si, F. Steglich, Heavy fermions and quantum phase transitions. *Science* **329**, 1161–1166 (2010). doi:10.1126/science.1191195 Medline
16. S. Paschen, T. Lühmann, S. Wirth, P. Gegenwart, O. Trovarelli, C. Geibel, F. Steglich, P. Coleman, Q. Si, Hall-effect evolution across a heavy-fermion quantum critical point. *Nature* **432**, 881–885 (2004). doi:10.1038/nature03129 Medline
17. A. Schröder, G. Aeppli, R. Coldea, M. Adams, O. Stockert, H. v. Löhneysen, E. Bucher, R. Ramazashvili, P. Coleman, Onset of antiferromagnetism in heavy-fermion metals. *Nature* **407**, 351–355 (2000). doi:10.1038/35030039 Medline
18. P. Gegenwart, C. Langhammer, C. Geibel, R. Helfrich, M. Lang, G. Sparn, F. Steglich, R. Horn, L. Donnevert, A. Link, W. Assmus, Breakup of Heavy Fermions on the Brink of "Phase A" in $CeCu_2Si_2$. *Phys. Rev. Lett.* **81**, 1501–1504 (1998). doi:10.1103/PhysRevLett.81.1501
19. J. Custers, P. Gegenwart, H. Wilhelm, K. Neumaier, Y. Tokiwa, O. Trovarelli, C. Geibel, F. Steglich, C. Pépin, P. Coleman, The break-up of heavy electrons at a quantum critical point. *Nature* **424**, 524–527 (2003). doi:10.1038/nature01774 Medline
20. A. B. Pippard, *Magnetoresistance in metals* (Cambridge University Press, 2009).
21. Supplementary materials.
22. S. Singh, C. Capan, M. Nicklas, M. Rams, A. Gladun, H. Lee, J. F. Ditusa, Z. Fisk, F. Steglich, S. Wirth, Probing the quantum critical behavior of $CeCoIn_5$ via Hall effect measurements. *Phys. Rev. Lett.* **98**, 057001 (2007). doi:10.1103/PhysRevLett.98.057001 Medline
23. L. D. Pham, T. Park, S. Maquilon, J. D. Thompson, Z. Fisk, Reversible tuning of the heavy-fermion ground state in $CeCoIn_5$. *Phys. Rev. Lett.* **97**, 056404 (2006). doi:10.1103/PhysRevLett.97.056404 Medline
24. Q. Y. Chen, X. B. Luo, E. Vescovo, K. Kaznatcheev, F. J. Walker, C. H. Ahn, Z. F. Ding, Z. H. Zhu, L. Shu, Y. B. Huang, J. Jiang, Electronic structure study of $LaCoIn_5$ and its comparison with $CeCoIn_5$. *Phys. Rev. B* **100**, 035117 (2019). doi:10.1103/PhysRevB.100.035117
25. K. Chen, F. Strigari, M. Sundermann, Z. Hu, Z. Fisk, E. D. Bauer, P. F. S. Rosa, J. L. Sarrao, J. D. Thompson, J. Herrero-Martin, E. Pellegrin, D. Betto, K. Kummer, A. Tanaka, S. Wirth, A. Severing, Evolution of ground-state wave function in $CeCoIn_5$ upon Cd or Sn doping. *Phys. Rev. B* **97**, 045134 (2018). doi:10.1103/PhysRevB.97.045134
26. A. Koitzsch, S. V. Borisenko, D. Inosov, J. Geck, V. B. Zabolotnyy, H. Shiozawa, M. Knupfer, J. Fink, B. Büchner, E. D. Bauer, J. L. Sarrao, R. Follath, Hybridization effects in $CeCoIn_5$ observed by angle-resolved photoemission. *Phys. Rev. B* **77**, 155128 (2008). doi:10.1103/PhysRevB.77.155128
27. S. Jang, J. D. Denlinger, J. W. Allen, V. S. Zapf, M. B. Maple, J. N. Kim, B. G. Jang, J. H. Shim, Evolution of the Kondo lattice electronic structure above the transport coherence temperature. *Proc. Natl. Acad. Sci. U.S.A.* **117**, 23467–23476 (2020). doi:10.1073/pnas.2001778117 Medline
28. N. Gauthier, J. A. Sobota, M. Hashimoto, H. Pfau, D.-H. Lu, E. D. Bauer, F. Ronning, P. S. Kirchmann, Z.-X. Shen, Quantum-well states in fractured crystals of the heavy-fermion material $CeCoIn_5$. *Phys. Rev. B* **102**, 125111 (2020). doi:10.1103/PhysRevB.102.125111
29. N. J. Curro, B. Simovic, P. C. Hammel, P. G. Pagliuso, J. L. Sarrao, J. D. Thompson, G. B. Martins, Anomalous NMR magnetic shifts in $CeCoIn_5$. *Phys. Rev. B* **64**, 180514(R) (2001). doi:10.1103/PhysRevB.64.180514
30. S. Fujimori, Band structures of 4*f* and 5*f* materials studied by angle-resolved photoelectron spectroscopy. *J. Phys. Condens. Matter* **28**, 153002 (2016). doi:10.1088/0953-8984/28/15/153002 Medline
31. Q. Y. Chen, D. F. Xu, X. H. Niu, J. Jiang, R. Peng, H. C. Xu, C. H. P. Wen, Z. F. Ding, K. Huang, L. Shu, Y. J. Zhang, H. Lee, V. N. Strocov, M. Shi, F. Bisti, T. Schmitt, Y. B. Huang, P. Dudin, X. C. Lai, S. Kirchner, H. Q. Yuan, D. L. Feng, Direct observation of how the heavy-fermion state develops in $CeCoIn_5$. *Phys. Rev. B* **96**, 045107 (2017). doi:10.1103/PhysRevB.96.045107
32. Q. Y. Chen, F. Ronning, E. D. Bauer, C. H. P. Wen, Y. B. Huang, D. L. Feng, Suppression of hybridization by Cd doping in $CeCoIn_5$. *Phys. Rev. B* **100**, 235148 (2019). doi:10.1103/PhysRevB.100.235148
33. K. Gofryk, F. Ronning, J.-X. Zhu, M. N. Ou, P. H. Tobash, S. S. Stoyko, X. Lu, A. Mar, T. Park, E. D. Bauer, J. D. Thompson, Z. Fisk, Electronic tuning and uniform superconductivity in $CeCoIn_5$. *Phys. Rev. Lett.* **109**, 186402 (2012). doi:10.1103/PhysRevLett.109.186402 Medline
34. H. Sakai, F. Ronning, J.-X. Zhu, N. Wakeham, H. Yasuoka, Y. Tokunaga, S. Kambe, E. D. Bauer, J. D. Thompson, Microscopic investigation of electronic inhomogeneity induced by substitutions in a quantum critical metal $CeCoIn_5$. *Phys. Rev. B* **92**, 121105 (2015). doi:10.1103/PhysRevB.92.121105
35. L. B. Ioffe, A. I. Larkin, Gapless fermions and gauge fields in dielectrics. *Phys. Rev. B* **39**, 8988–8999 (1989). doi:10.1103/PhysRevB.39.8988 Medline
36. A. Banerjee, P. Lampen-Kelley, J. Knolle, C. Balz, A. A. Aczel, B. Winn, Y. Liu, D. Pajerowski, J. Yan, C. A. Bridges, A. T. Savici, B. C. Chakoumakos, M. D. Lumsden, D. A. Tennant, R. Moessner, D. G. Mandrus, S. E. Nagler, Excitations in the field-induced quantum spin liquid state of α-$RuCl_3$. *NPJ Quant. Mater.* **3**, 8 (2018). doi:10.1038/s41535-018-0079-2
37. T. Senthil, M. P. A. Fisher, Detecting fractions of electrons in the high-T_c cuprates. *Phys. Rev. B* **64**, 214511 (2001). doi:10.1103/PhysRevB.64.214511
38. S. Badoux, W. Tabis, F. Laliberté, G. Grissonnanche, B. Vignolle, D. Vignolles, J. Béard, D. A. Bonn, W. N. Hardy, R. Liang, N. Doiron-Leyraud, L. Taillefer, C. Proust, Change of carrier density at the pseudogap critical point of a cuprate superconductor. *Nature* **531**, 210–214 (2016). doi:10.1038/nature16983 Medline
39. Data and materials, doi: 10.17605/OSF.IO/DFM7X.
40. P. Blaha, K. Schwarz, F. Tran, R. Laskowski, G. K. H. Madsen, L. D. Marks, WIEN2k: An APW+lo program for calculating the properties of solids. *J. Chem. Phys.* **152**, 074101 (2020). doi:10.1063/1.5143061 Medline
41. J. Kuneš, P. Novák, M. Diviš, P. M. Oppeneer, Magnetic, magneto-optical, and structural properties of URhAl from first-principles calculations. *Phys. Rev. B* **63**, 205111 (2001). doi:10.1103/PhysRevB.63.205111
42. J. P. Perdew, Y. Wang, Accurate and simple analytic representation of the electron-gas correlation energy. *Phys. Rev. B* **45**, 13244–13249 (1992). doi:10.1103/PhysRevB.45.13244 Medline
43. S. Elgazzar, I. Opahle, R. Hayn, P. M. Oppeneer, Calculated de Haas–van Alphen quantities of $CeMIn_5$ (M = Co, Rh, and Ir) compounds. *Phys. Rev. B* **69**, 214510 (2004). doi:10.1103/PhysRevB.69.214510
44. P. M. C. Rourke, S. R. Julian, Numerical extraction of de Haas–van Alphen frequencies from calculated band energies. *Comput. Phys. Commun.* **183**, 324–332 (2012). doi:10.1016/j.cpc.2011.10.015

ACKNOWLEDGMENTS

We would like to thank C. Varma, S. Sachdev, S. Chatterjee, M. Vojta, and J. D. Denlinger for helpful discussions. We thank E. Green for support during experiments at the milliKelvin facility at the National High Magnetic Field Lab. Hall bar devices were fabricated at the Focused Ion Beam at the National Center for Electron Microscopy Sciences at Lawrence Berkeley National Laboratory. **Funding:** This work was supported by the U.S. Department of Energy, Office of Science, Basic Energy Sciences, Materials Sciences and Engineering Division under Contract No. DE-AC02-05-CH11231 within the Quantum Materials program (KC2202). V.N., T.C., and D.H.E. are supported by the National Science Foundation Graduate Research Fellowship Grant No. DGE-1752814. This work was partially supported by the Gordon and Betty Moore Foundations EPiQS Initiative through Grant GBMF9067. P.M.O. and J.R. are supported by the Swedish Research Council (VR), and the K. and A. Wallenberg Foundation Award No. 2015.0060. DFT calculations have been performed using resources of Swedish National Infrastructure for Computing (SNIC) at the NSC center (cluster Tetralith). Pulsed field and dilution fridge experiments were collected at the National High Magnetic Field Laboratories in Tallahassee, Florida, and Los Alamos, New Mexico respectively, which are supported by the National Science Foundation Cooperative Agreement No. DMR-1644779 and the State of Florida. **Author contributions:** N.M, I.M.H., and F.W. performed continuous field Hall effect measurements. N.M. and V.N. performed the quantum oscillation experiments. N.M., S.F., F.W., S.J. and A.G. grew the samples and performed heat capacity and magnetization measurements. T.C., Y.W., and E.A. performed theoretical calculations of the Hall coefficient. J.R. and P.M.O. performed DFT simulations of Fermi surface topologies and dHvA oscillation frequencies. S.C.H and E.M. fabricated Hall bar devices for pulsed field measurements. A.B.

performed dilution fridge measurements. J.S., J.C.P., L.W., and R.M. performed pulsed field measurements. D.H.E., P.A, Y.L, S.C, and J.G. performed ARPES measurements. All authors contributed to writing the manuscript. **Competing interests:** The authors declare no competing financial interests. **Data and materials availability:** All data provided in this report are publicly available: https://osf.io/dfm7x/ (*39*).

SUPPLEMENTARY MATERIALS
science.org/doi/10.1126/science.aaz4566
Materials and Methods
Supplementary Text
Figs. S1 to S16
References (*40*–*44*)

10 September 2019; resubmitted 18 June 2020
Accepted 15 November 2021
Published online 2 December 2021
10.1126/science.aaz4566

Table 1. de Haas-van Alphen extremal orbit assignments. Units of kiloTesla, H || [001], from experiments and DFT calculations. Each orbit is labeled by the assigned Fermi surface sheet, which are visualized on the calculated Fermi surface sheets in Fig. 2A.

Fermi surface	dHvA orbit label	localized *f*-electron model	$CeCoIn_5$ Ref. (*5*)	0.33% Sn-doped $CeCoIn_5$	delocalized *f*-electron model
γ_Z	γ_1	0.8			
γ_Z	γ_2	2.3			
γ-cross	γ_3	13.2			
γ-ellipsoid	γ_4			(0.46)	0.7
γ-ellipsoid	γ_5		(0.24)	(0.2)	0.22
α-cylinder	α_1	4.8	5.6	5.4	5.6
α-cylinder	α_2	4.0	4.5	4.8	4.4
α-cylinder	α_3	3.9	4.2	4.4	4.3
α_Z	α_4			16.3	15.8
β-cylinder	β_1	10.3	12.0	11.9	12.3
β-cylinder	β_2	6.1	7.5	6.8	6.7
β_Z/cylinder	β_3			2.0	1.6
β_Z/cylinder	β_4			1.2	0.9

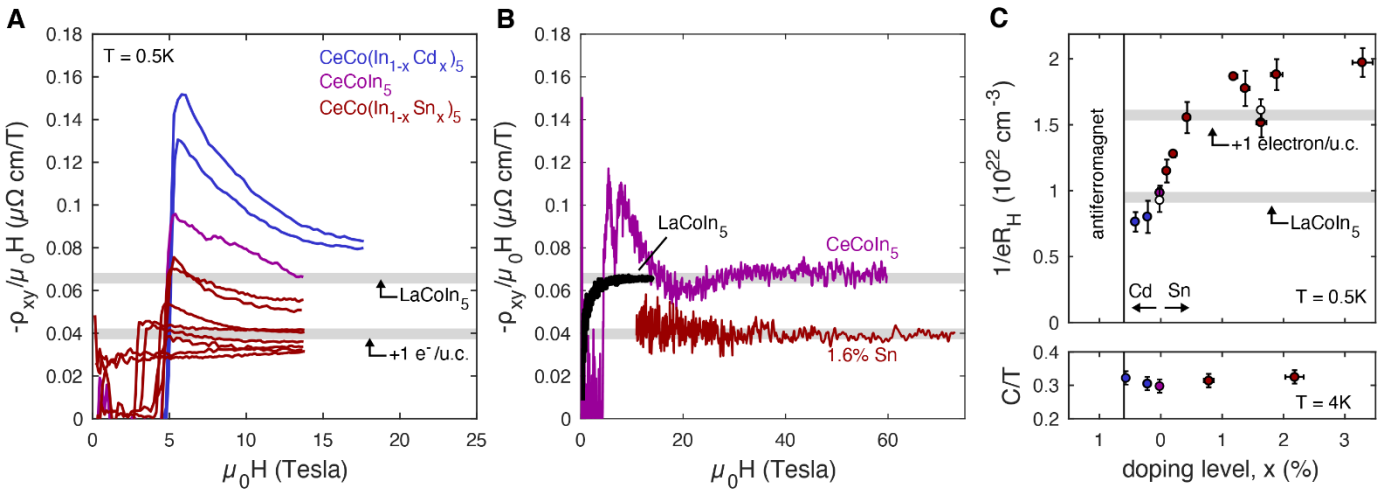

Fig. 1. Carrier density measurements in doped $CeCoIn_5$. (**A**) Hall coefficient as a function of field in doped $CeCoIn_5$ with Cd concentrations 0.2% and 0.4%, and Sn concentrations 0.11%, 0.22%, 0.33%, 0.44%, 1.2%, 1.39%, 1.65%, 1.9%, and 3.3%. As discussed in the main text, the inverse of the Hall coefficient $\left(\rho_{xy} / \mu_0 H\right)$ in the high-field limit can be used to approximate the net carrier density (see also (*21*) Section 4). Gray lines denote the high-field Hall coefficient of the non-*f* analog $LaCoIn_5$ and the calculated value including one additional electron per unit cell. (**B**) Pulsed field Hall resistivity of $CeCoIn_5$ (T = 0.66 K) and Sn-doped $CeCoIn_5$ (T = 0.5 K) overlaid on the continuous field Hall resistivity of $LaCoIn_5$ (1.8 K). (**C**) Inverse high-field Hall coefficient of $CeCoIn_5$ at 0.5 K as a function of doping level, including measurements in continuous field up to 14 T or 18 T (filled circles) and pulsed field up to 73 T (open circles). With Sn-substitution, the apparent carrier density of $CeCoIn_5$ increases by about one electron per unit cell above that of $LaCoIn_5$. This trend provides evidence that Sn-substitution delocalizes the single cerium *f*-electron per unit cell in $CeCoIn_5$. The value of $1/eR_H$ in some Sn-doped samples lies above the calculated +1 electron line, likely because the Hall coefficient has not completely saturated in these samples at 14 T. At higher fields the value of $1/eR_H$ seems to saturate at the +1 electron value as seen in the 1.6% Sn-doped sample at 70 T. The lower panel shows the 4 Kelvin heat capacity (units of mJ/mol K^2) across this doping series.

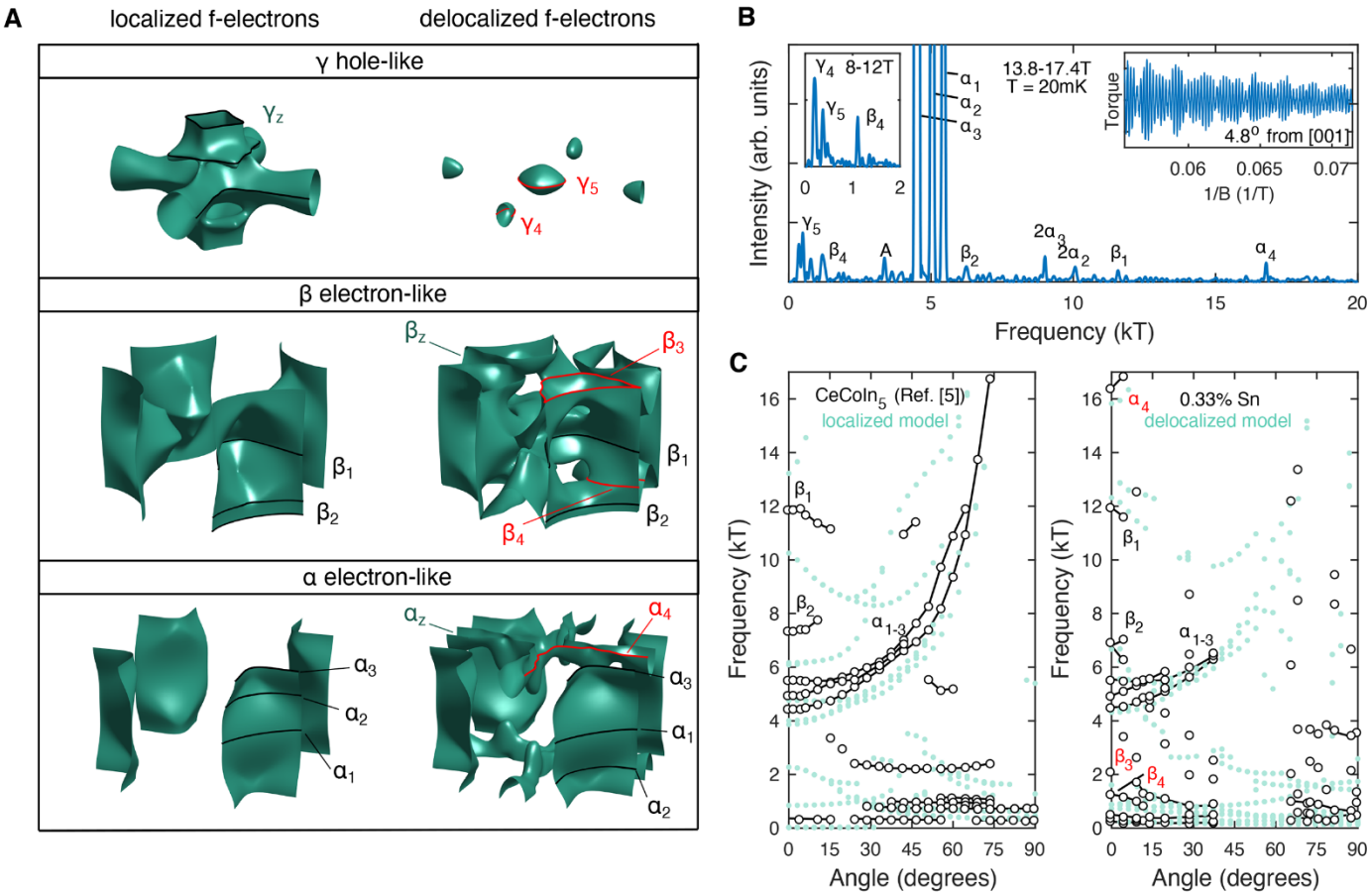

Fig. 2. de Haas-van Alphen oscillations in Sn-doped $CeCoIn_5$ and comparison to DFT calculations. (**A**) DFT calculated Fermi surface sheets of $CeCoIn_5$ with localized and delocalized *f*-electron models. Predicted dHvA orbits for $H \parallel [001]$ are drawn in black and red. Red orbits are unique to the delocalized *f*-electron model. (**B**) Characteristic dHvA spectrum with the magnetic field 4.8° away from [001] of a crystal of 0.33% Sn-doped $CeCoIn_5$. The inset shows oscillations in the magnetic torque after background subtraction. (**C**) dHvA oscillation frequencies as a function of angle tilting the magnetic field from the crystallographic [001] to [100] directions in pure $CeCoIn_5$ (Ref. (*5*)) and 0.33% Sn-doped $CeCoIn_5$. Light green points are DFT calculated frequencies of the localized and delocalized *f*-electron models respectively.

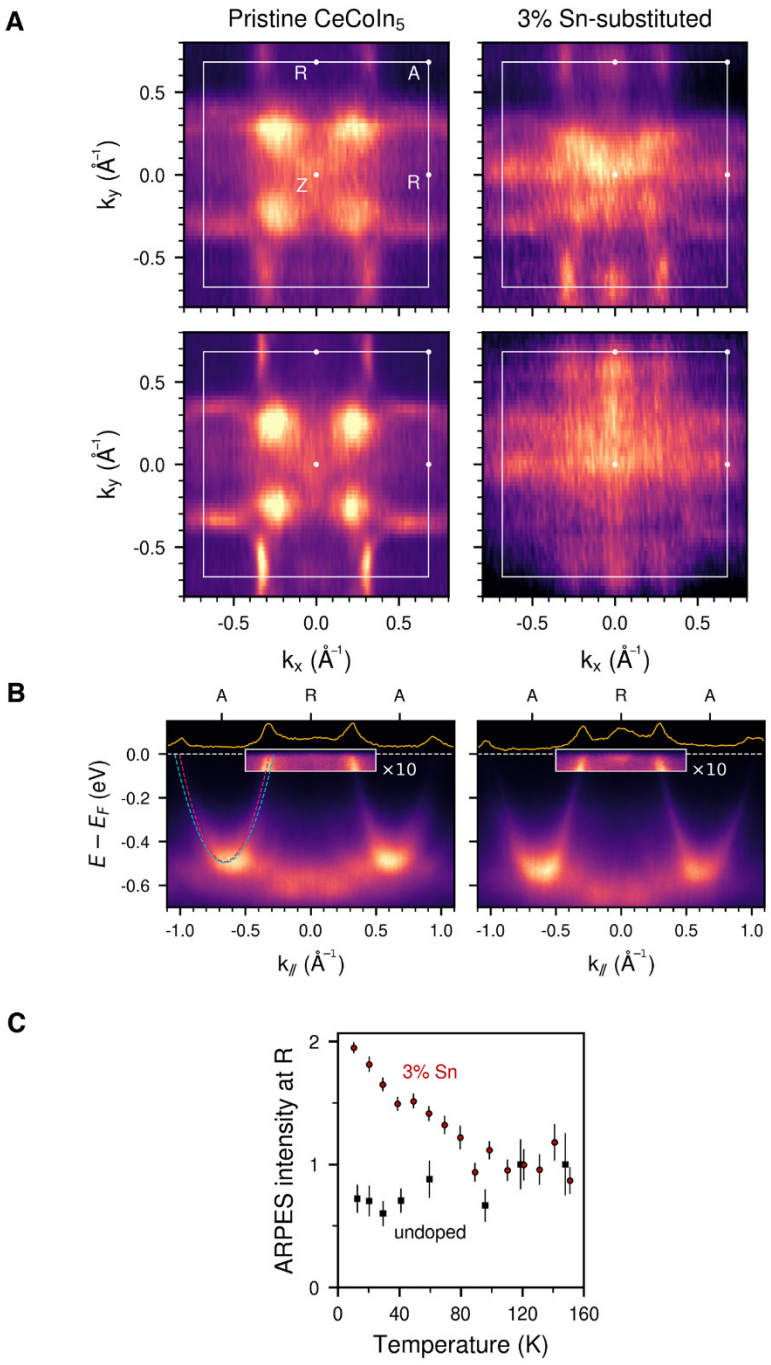

Fig. 3. ARPES measurements of $CeCoIn_5$ and Sn-doped $CeCoIn_5$. (**A**) Fermi surface maps in pure and 3% Sn-substituted $CeCoIn_5$ at the Brillouin zone top (RZA plane). A new Fermi surface sheet appears at the zone top in the Sn-substituted sample. Each of the four subpanels represents measurements on a different cleave. (**B**) A-R-A dispersion cuts. Parabolic α and β bands are labeled by red and blue dotted lines. The new Fermi surface in the Sn-substituted sample is observed as an increase in spectral intensity at the Fermi level at R. The spectral intensity within the white box has been enhanced by a factor of ten for clarity. (**C**) Comparison of temperature-dependent intensity at the R point normalized to the average value between 120-160 K.

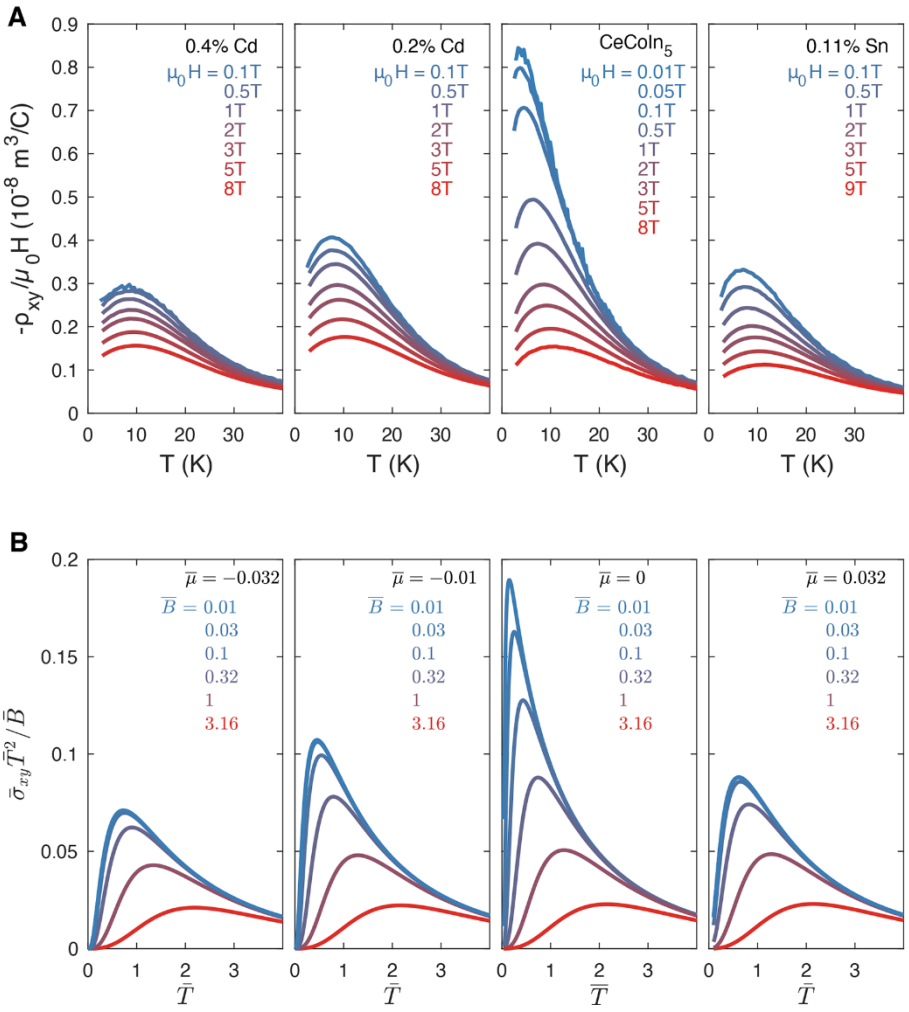

Fig. 4. Comparison of experimental data and theoretical calculations of the conductivity of critical valence fluctuations around an *f*-electron delocalization transition. (**A**) Experimentally measured Hall resistivity, divided by the applied magnetic field, for samples with different compositions. (**B**) The theoretically predicted Hall effect from bosonic valence fluctuations of the fractionalized Fermi liquid model. Each panel is labeled by the chemical potential in the theory corresponding to the doping level in the experiment, where $\mu < 0$ corresponds to hole-doping and $\mu > 0$ corresponds to electron-doping. Curves are labeled by the normalized magnetic field value and all theory data includes a parametrization of impurity scattering, $\bar{C} = 4$. See Supplement S7 (*21*) for the details of the calculation and relevant parameter normalizations.